Extraction of Particle Residence Time using echo-Lagrangian particle tracking

Mark D. Jeronimo[1]*, **Mohammad Reza Najjari**[1], **Kai Zhang**[1], **David E. Rival**[1]

[1] Queen's University, Department of Mechanical and Materials Engineering, Kingston, Canada

* mark.jeronimo@queensu.ca

Abstract

Eulerian, ultrasound-based velocimetry has become a popular tool for evaluating non-optically accessible flows and has demonstrated great potential for medical applications. This study presents a method of extracting path-dependent dynamics from time-resolved ultrasound images: echo-Lagrangian particle tracking (echoLPT). Ultrasound imaging can suffer from low signal-to-noise ratios and particle ambiguity. Material choices, image optimization and particle image enhancement techniques, and how they influence particle detection and tracking, are detailed. Thousands of flow tracers are tracked and the path each follows is revealed from the moment it enters the measurement domain. Knowledge of particle history allows the Particle Residence Time to be calculated for specific particles and regions of interest. Particle Residence Time, obtained from echoLPT, is compared for various pulsatile flow profiles through an idealized stenosis model. The Reynolds number, Womersley number and amplitude ratio of the pulsatile waveforms ranged from 32 to 128, 15 to 20 and 0.5 to 1.0, respectively, and echoLPT quantifies the effect of each.

1 Introduction

The concept of particle tracking has been long established as an effective flow visualization technique, but remains underdeveloped as a tool for evaluating non-optically accessible flows. Particle tracking velocimetry, or PTV (conceived by Adamczyk and Rimai (1988)), uses a Lagrangian reference frame to track the position of fluid parcels through time. This allows path-dependent dynamics to be evaluated; information that is lost to Eulerian field measurements typical of particle image velocimetry (PIV). However, flow field measurement using PIV (Adrian and Westerweel, 2011) was quickly recognized as a valuable tool, particularly for its ability to measure turbulent coherent structures, and overshadowed PTV. While both techniques have seen continual development to date, PIV remains the de facto standard for high spatial and temporal resolution flow measurements. State-of-the-art techniques, like tomographic PIV (Scarano, 2013) and Shake-The-Box (STB) (Schanz et al., 2016), have drastically improved particle image density and accuracy over their predecessors, but are impractical and overly complex for many experimental studies. Furthermore, the measurements are constrained to optically-accessible flows. An opaque vessel or dispersed phase can render these techniques ineffective and severely limit their application, e.g. *in vivo* or two-phase industrial flows.

In recent years, non-optical ultrasound imaging velocimetry (UIV), or echo-PIV, was introduced (Crapper et al., 2000; Kim et al., 2004) to evaluate sediment-laden (Crapper et al., 2000; Zheng et al., 2006) and cardiovascular flows (Zhang et al., 2011; Walker et al., 2014; Sampath et al., 2018). Despite the development (Poelma, 2017) that ultrasound-based velocimetry has seen, and the incorporation of PTV to improve field measurements (Sampath et al., 2018), there is still no Lagrangian-based ultrasound tool akin to PTV for optical measurements. Most recently, Ackermann and Schmitz (2016) and Song et al. (2018) have developed an ultrasonic method for tracking the movement of a contrast agent through *in vivo* microvessels. While their techniques reveal the position and velocity of microbubbles that can be used to describe the anatomy of the micro-vascular network, their movement is confined to minuscule channels that limit the conclusions that can be drawn about the actual flow physics. In larger vessels, path-dependent hemodynamics are not clearly understood, especially in the presence of cardiovascular complications like stenoses and aneurysms, and require a Lagrangian perspective to properly understand the flow-derived risk factors.
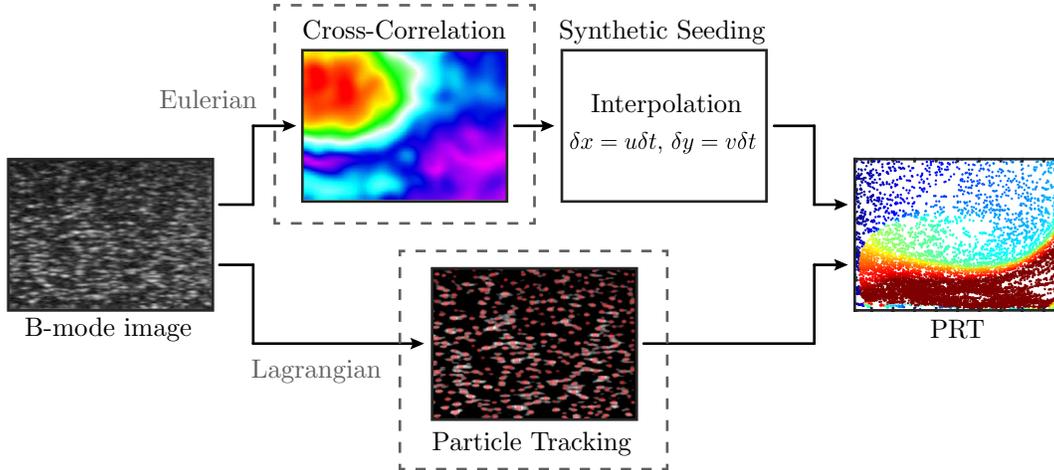
Figure 1: Path-dependent variables, like PRT, can be derived from both Eulerian and Lagrangian methods. The method described herein demonstrates how the more direct Lagrangian approach can be accomplished using ultrasound imaging.

Ultrasound-based particle tracking and path-dependent dynamics have many immediate applications over a broad range of fluid scales, including the study of multi-phase or sediment-laden flows, and understanding the intricacies of blood flow through diseased vessels. One such Lagrangian metric is Particle Residence Time (PRT), which is defined as the time a fluid parcel spends in a region of interest. PRT has been shown to link to increased plaque deposition and promote thrombogenesis and atherosclerosis in large blood vessels (Tambasco and Steinman, 2003). Figure 1 shows two approaches for measuring PRT from ultrasound images. Current UIV techniques (Eulerian) require the additional step of synthetically seeding the computed velocity field to map particle displacements and calculate PRT. A Lagrangian approach, however, provides a direct path to the same information (Figure 1), as evidenced by Jeronimo et al. (2019) for optical data. In this study a procedure, coined echo-Lagrangian particle tracking (echoLPT), is described to extract Lagrangian metrics from time-resolved ultrasound images. As a proof of concept, PRT within a post-stenotic recirculation region is measured by echoLPT and compared for varying flow conditions.

2 Methodology

2.1 Experimental setup

Experiments were performed in a table-top flow loop. A piston pump drives flow laden with ultrasonic contrast agent through an acrylic pipe with an inner diameter (D) of 22.225 mm and wall thickness of 1.6 mm. Approximately $100D$ downstream of the pipe entrance is a 3D-printed, idealized stenosis model consisting of a smooth contraction of the flow loop's internal pipe diameter, followed by a sudden expansion. The diametrical contraction of the stenosis wall follows the smooth sinusoidal curve given by y for $-0.5 \leq x/L < 0$:

$$y(x) = \frac{1}{2}\left[d + (D - d)\sin^2\left(\frac{\pi x}{2L}\right)\right], \tag{1}$$

where x is the distance along the pipe, $d = D/2$ is the diameter of the stenosis throat, and $L = 22.225$ mm is the length of the stenosis model. The stenosis geometry creates a recirculation region immediately downstream of the expansion, and is one of many poorly understood *in vivo* geometries that would be targeted for Lagrangian tracking analysis. Flow through the stenosis was generated using a physiological pump (CompuFlow 1000, Shelley Medical Systems). To evaluate echo-Lagrangian particle tracking, PRT was measured and compared for various pulsatile flow profiles. The pulsatile waveforms are the sum of steady and oscillatory (sinusoidal) flows, where the steady component defines the mean Reynolds number (Re_m) and the oscillatory component specifies the frequency of pulsation (f_p) and amplitude ratio, $\lambda = Re_o/Re_m$, where Re_o is the Reynolds number of the oscillatory component. Three Reynolds numbers were compared ($Re_m = 32$, 64 and 128), as well as two amplitudes ($\lambda = 0.5$ and 1.0). Two values of the Womersley number
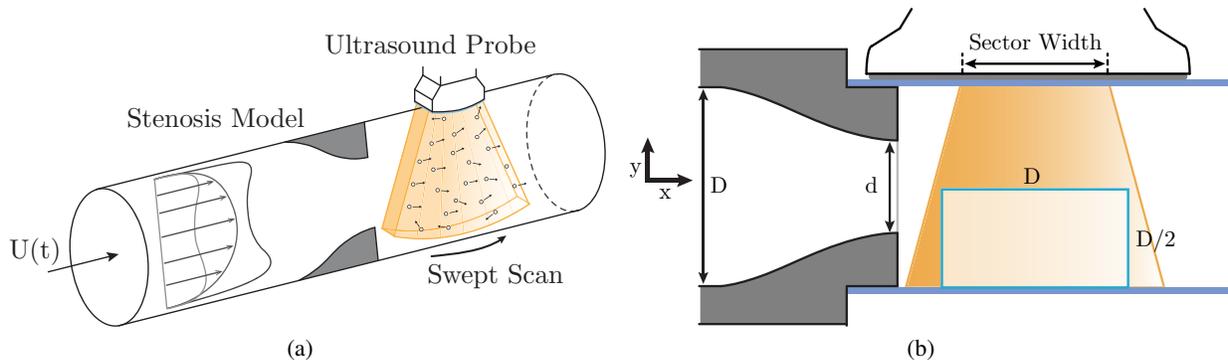
Figure 2: (a) Schematic of pulsatile flow, $U(t)$, through an axisymmetric stenosis model. A linear-array ultrasound transducer situated at the stenosis exit records the motion of microbubbles suspended in the fluid. (b) Cross-section of the stenosis and field-of-view. The sector width of ultrasound beam is set to 50% to maximize the acquisition rate, but shifts the measurement domain (blue outline) away from the wall of stenosis.

$(\alpha = D/2\sqrt{2\pi f_p/\nu})$, a dimensionless group commonly used to characterize pulsatile flows (Womersley, 1955) and a function of f_p, were chosen ($\alpha = 15$ and 20) for their relevance to cardiovascular flows. The working fluid, an aqueous solution with 40% w/w glycerol, has a kinematic viscosity, ν, of 3.4×10^{-6} m^2/s.

An ultrasound probe acts as a transmitter of high frequency sound waves and receiver of the reflected signals, referred to as echoes. A 128-element linear-array ultrasound transducer (BK Medical) is aligned with the centreline of the pipe and affixed just downstream of the stenosis model. The test section of the acrylic pipe, including the stenosis and transducer head, is submerged in water to avoid a large change in acoustic impedance that would strongly reflect sound waves should they pass through air. The choice of pipe material should be made to minimize the differences in the acoustic impedances of each medium the incident waves must cross; acrylic and elastomeric materials (e.g., Sylgard-184) have impedances very close to that of the working fluid and the intensity of signals reflected at the wall-fluid interfaces is small. Additionally, care must be taken to choose a material that does not strongly attenuate sound waves. A Sylgard-184 model was discarded in favour of acrylic because the former has a much greater attenuation coefficient. Despite these precautions, the strength of the transmitted signal is still substantially weakened – considerably so when compared to an equivalent optical setup – and there are bright reflection artifacts near the upper wall of the test section. As a result, the measurement domain is refined to extend from the bottom wall to the centreline of the pipe ($D/2$) and approximately one diameter (D) axially.

2.2 Contrast imaging

To extract Lagrangian information from the flow it is seeded with an ultrasound contrast agent that faithfully follow the flow and exhibit very high echogenicity. Definity microbubbles (Lantheus Medical Imaging) are lipid-encapsulated perfluoropropane bubbles that are developed for ultrasound imaging. These micrometre-sized bubbles have very high acoustic impedance and strongly reflect sound waves. Compared to medical applications, where large volumes of contrast are used to effectively illuminate blood flow, the concentration of the contrast-enhancing agent must be carefully controlled for fluids research. UIV studies have evaluated the effect of contrast agent concentration on velocimetry results and quote values in the range 800 2000 bubbles/mL for *in vitro* experiments (Kim et al., 2004; Niu et al., 2011). For the purpose of microbubble tracking, the concentration is reduced to approximately 500 bubbles/mL, or 225 bubbles in the measurement domain. EchoLPT is highly sensitive to particle image density, much more so than UIV. A high concentration of microbubbles lowers the quality of particle detection by increasing particle image ambiguity – an issue that is exacerbated by variability of the point spread function that distorts tracer images (Ortiz et al., 2012). This compounds to jeopardize successful tracking and decreases the mean track length. Walker et al. (2014) had difficulty observing microbubbles in the recirculation zone immediately behind a stenosis geometry and speculated that the bubbles did not follow the flow into those regions. In this study, manipulation of the power of the transmitted signal revealed flow tracers within the near-wall region. It was found that reducing the power prevented microbubbles from bursting in regions of extended ultrasound

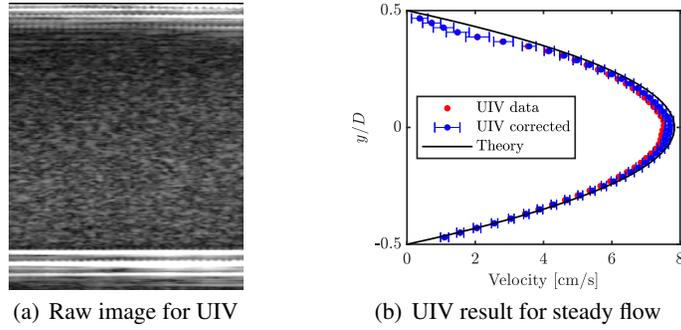(a) Raw image for UIV

(b) UIV result for steady flow

Figure 3: (a) Example of a raw image used for UIV. The particle image density is higher than what is usable for tracking. (b) UIV results compared to the theoretical, Hagen-Poiseuille solution for steady flow through a straight pipe. The ability to match this profile and the errors associated verify the quality of the ultrasound-based measurements in this study.

exposure; increasing the power would quickly reduce the bubble concentration in the bottom of the pipe. Apart from the power settings, the frequency, line density and sector width of the emitted sound waves, and the gain and dynamic range of the received signal were all adjusted to optimize the brightness-mode (B-mode) images for echoLPT. The frequency, gain and dynamic range of the ultrasound system control image quality, where quality is judged by particle image shape and contrast, i.e. signal-to-noise ratio. For a given scan depth, the transducer's line density and sector width directly influence the frame rate. Here, a maximal frame rate of 173 Hz was achieved by setting the sector width to a minimum (50%) and the line density to 192 to retain good lateral resolution. The frame rate was a limiting factor on the flow profiles evaluated, and Re_m and λ were chosen to constrain frame-to-frame bubble displacement to 12 pixels. Finally, the ultrasound beam has a thickness of approximately 2 mm (10% of the diameter of the pipe) so this two-dimensional technique is actually operating on a volume. However, Jeronimo et al. (2019) showed that thick-sheet measurements can minimize particle loss due to out-of-plane motion without contributing significantly to tracking error.

2.3 UIV validation

To validate our ultrasound setup for flow measurement, B-mode images of steady flows through a section of straight pipe upstream of the stenosis model were collected and compared to a theoretical Hagen-Poiseuille profile using ultrasound image velocimetry. Figure 3 shows the mean velocity profile calculated by UIV using a sliding sum-of-correlation algorithm and 24×24 pixel interrogation windows with 75% overlap. The computed velocities are scan corrected (Poelma, 2017) and match the theoretical parabolic profile within 5%. The result of the UIV experiment gives confidence to our procedure and quality of ultrasound images for Lagrangian analysis.

2.4 B-mode image preprocessing

Figure 4(a) shows an example of a B-mode image collected for echoLPT. Compared to Figure 3(a), the particle image density is visibly lower and individual particles are easily identified. The aforementioned ultrasonic reflections near the top of the field of view are apparent and a smaller domain (outlined in blue in Figure 4(b)) was selected for measurements. Despite tuning the B-mode images, the signal-to-noise ratio is low and images must be thoroughly filtered before the detection and tracking processes. First, images are scaled using the sector width (50%), number of elements in the transducer (128) and horizontal pixel pitch of each element (0.3 mm) to compute the width of the field of view. Subtraction of the mean image intensity across all images removes stationary features, like strong reflections and noise, from the background of each frame. The images are then smoothed using a Gaussian smoothing filter, with a 9×9 pixel fit to account for large bubble images. The Gaussian filter rounds particles by smearing the peak intensity of each particle slightly. To refocus the particle images a sharpening filter is applied that reduces particle size once again to produce high contrast images. Figure 4(b) shows the result of the preprocessing steps. Due to thickness of the measurement plane and noise inherent of the ultrasound modality, there is still considerable variability

(a) Raw B-mode image   (b) Preprocessed image   (c) Detected particles
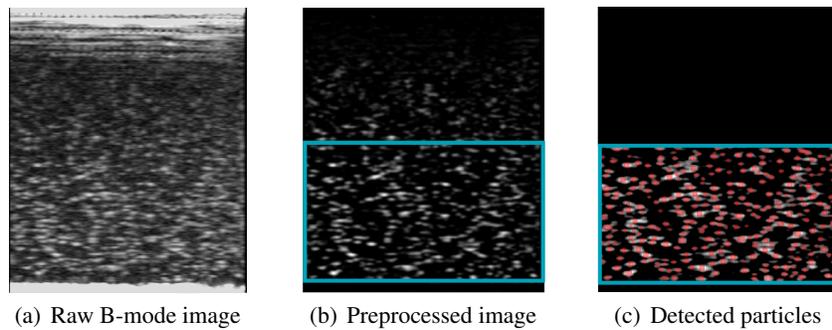
Figure 4: EchoLPT uses (a) low-seeding density B-mode images that are (b) preprocessed, using background and smoothing filters, to reduce particle image ambiguity and increase contrast. (c) Particles within the measurement domain are detected in each frame using peak detection. Detected particles are highlighted in red. The measurement domain is designated by a blue outline.

in the shape, size and intensity of particles. Each of these inconsistencies have been linked to errors in PIV measurements where they affect a particle image's contribution to the correlation function (Adrian and Westerweel, 2011; Raffel et al., 2018). Lagrangian tracking algorithms are not affected in this regard as they look for particle-specific matches from one frame to the next. The image enhancement methods described above were sufficient to effectively track microbubbles.

2.5 Echo-Lagrangian particle tracking

Path-dependent dynamics are extracted from the preprocessed images using echoLPT following three steps: particle detection, particle tracking and path extension. Particle detection is performed using simple peak thresholding based on a case-specific intensity threshold and particle fit mode to specify individual microbubble positions at each time step. In this study, an 11×11 Gaussian fit identifies large bubble images. This assigns a Gaussian shape to the peak intensity of distorted images, but was found to not affect the ability to track said particles. Figure 4(c) shows an overlay of the detected particles (red) on the filtered image. Detected particles are tracked from frame to frame using a peak-matching algorithm that searches within an allowable displacement range and maximum relative acceleration. The range is flow-specific and, because it is applied across the entire domain, can lead to erroneous matches for large dynamic ranges, e.g. a particle within a slow-moving recirculation may be assigned a non-physical velocity. Each particle's displacement is verified by checking the spatial coherence of particle velocities in its vicinity. Particles that find a match from one time step to the next are connected to form tracks. Particles that have no match are discarded. The pathlines produced are short, as is typical of optical PTV, so they must be extended to glean their full trajectory. Path extension follows the method described and implemented in Rosi and Rival (2018) and Jeronimo et al. (2019). Microbubble trajectories are predicted using flow maps that are fit to the scattered echoLPT data at each time step using a local weighted regression (loess) algorithm. Due to the sparsity of ultrasound images, the nearest 10% of the detected particles are used to fit the flow map at each location, as depicted in Figure 5(a). While particle ambiguity limits the seeding density for echoLPT, flow map compilation requires a minimum microbubble concentration – too low and the flow maps may experience strong gradients. Forwards- and backwards-time flow maps are used to extend each track to its terminal position and back to its source. A unique track for each detected microbubble contains time-resolved positional data. After extending the particle tracks they are filtered a final time: if any single step is greater than the original allowable displacement range then the entire track is deleted. To visualize the behaviour of microbubbles in the measurement domain, bubbles are assigned a colour label based on their trajectory downstream of the stenosis model (see Figure 5(b)).

3 Results

Over a recording period of five seconds (865 frames) an average of 50,000 unique microbubbles were tracked in each flow regime tested. The mean track length for those tracers was extended from only 4 frames to approximately 210 frames. Path extension increased the effective particle image density from 0.004 particles

(a) Track extension
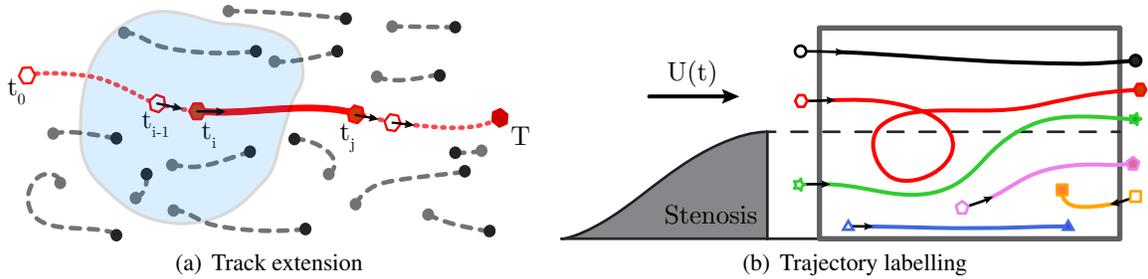
(b) Trajectory labelling

Figure 5: (a) Particle pathlines are extended forwards and backwards using flow maps fit to each time step using a lowess regression fit with the nearest 10% of particle images. A short track (solid red line) is extended to its full length (dotted red line) by drawing pathlines forwards to T and backwards to t_0. (b) Extended pathlines are colour-labelled based on their trajectory through the field of view. Black and red tracks enter the domain above the edge of the stenosis, but red particles experience significant mixing. Green and orange tracks enter from upstream and downstream, respectively, while blue and pink particles begin within the domain. Blue particles spend their entire lifetime in view and below the stenosis edge. Not to scale.

per pixel (ppp) to 0.150 ppp. The movement of the contrast agent through the measurement domain was evaluated qualitatively by colour-labelling based on each bubble's source and terminal positions. Figure 6 shows an example of trajectory-based labelling made possible by particle tracking and demonstrates the ability to follow individual microbubbles using ultrasound imaging. Of particular interest is the mixing of red and green particles, which enter the field of view above and below the level of the stenosis opening, respectively.

To evaluate the quantitative value of echoLPT the PRT of each particle that entered the measurement domain was calculated. PRT is a path-dependent quantity that has been measured as the length of time a particle spends within a region of interest. A microbubble's PRT increases as it spends time within the chosen region of interest, whether that is the entire measurement domain (Figure 7(a)) or a specific area (Figure 7(b)), e.g., within an aneurysm. By this method, the PRT of each particle is known at each instant in time, without any temporal or spatial averaging. The mean PRT for particles that enter one of the three demarcated regions in Figure 7(b) are 0.13 s (top), 0.88 s (bottom-left) and 1.20 s (bottom-right). If the movement of the particles is animated some jitter is apparent. The jitter is a result of changes to the particle image shape from frame to frame, which shifts the position of a particle's peak intensity. Fortunately, the resultant displacements are small (< 5 frames) and had no significant effect on PRT calculations. To demonstrate the insight that can be drawn from echoLPT, the red-labelled particles for varying Re_m, α and λ were compared by analyzing the probability distribution of their PRT. Figure 8 is the PRT distribution of red particles within the measurement domain for $Re_m = 64$. In the absence of pulsatility the red particles move steadily through the domain and the distribution is very narrow. Introducing an oscillatory component to the flow decreased the peak PRT in all cases, but increased variance. At each value of λ, increasing α narrows and shifts the distribution towards higher PRT, suggesting pulsatility promotes mixing into the recirculation region, prolonging the microbubbles' transit time. Conversely, a greater amplitude ratio caused a shift towards shorter PRT. Larger velocity gradients forced red particles through the measurement domain faster. Figure 9 clearly highlights the decrease in PRT as Re_m is increased, while also supporting the narrowing and positive shift of the distribution of red particle PRT as the pulse frequency rises.

4 Conclusions

After decades of development, optical PIV and PTV are now turnkey operations that are capable of revealing the fluid dynamics of incredibly complex flows from Eulerian and Lagrangian perspectives. In order to assess non-optically accessible flows, however, the same information is not as easily acquired. In this study, it is demonstrated that it is feasible to measure path-dependent dynamics in pulsatile flows without optical access using ultrasound-based Lagrangian particle tracking. The technique is shown to be an effective and accessible tool, but image capture and particle image detection each require careful tuning.
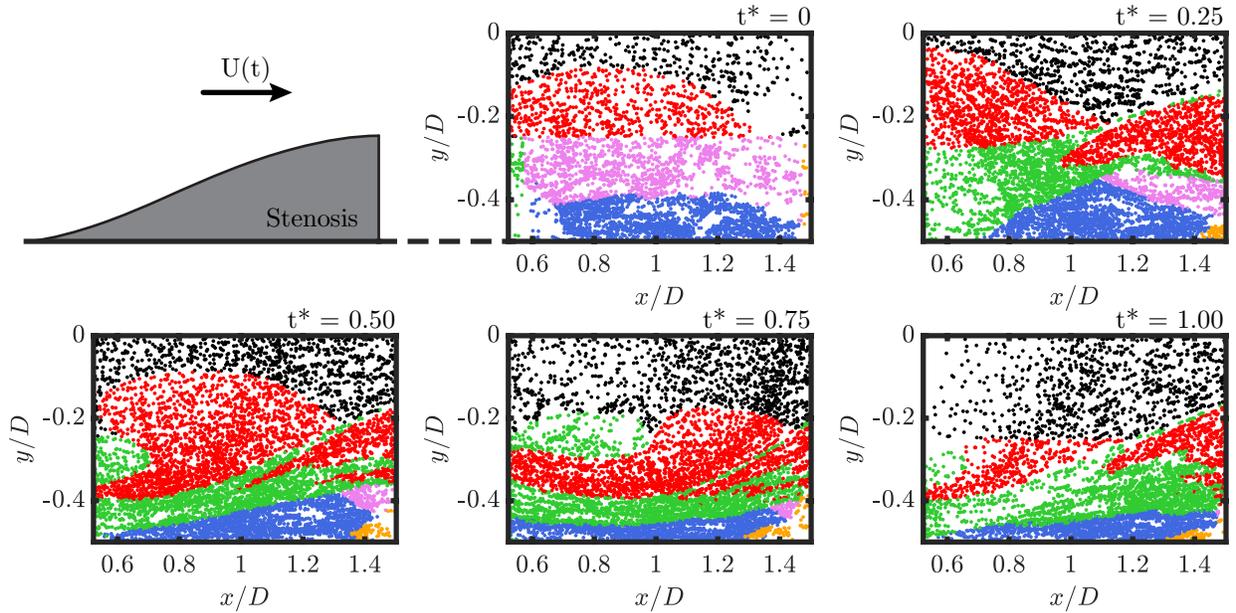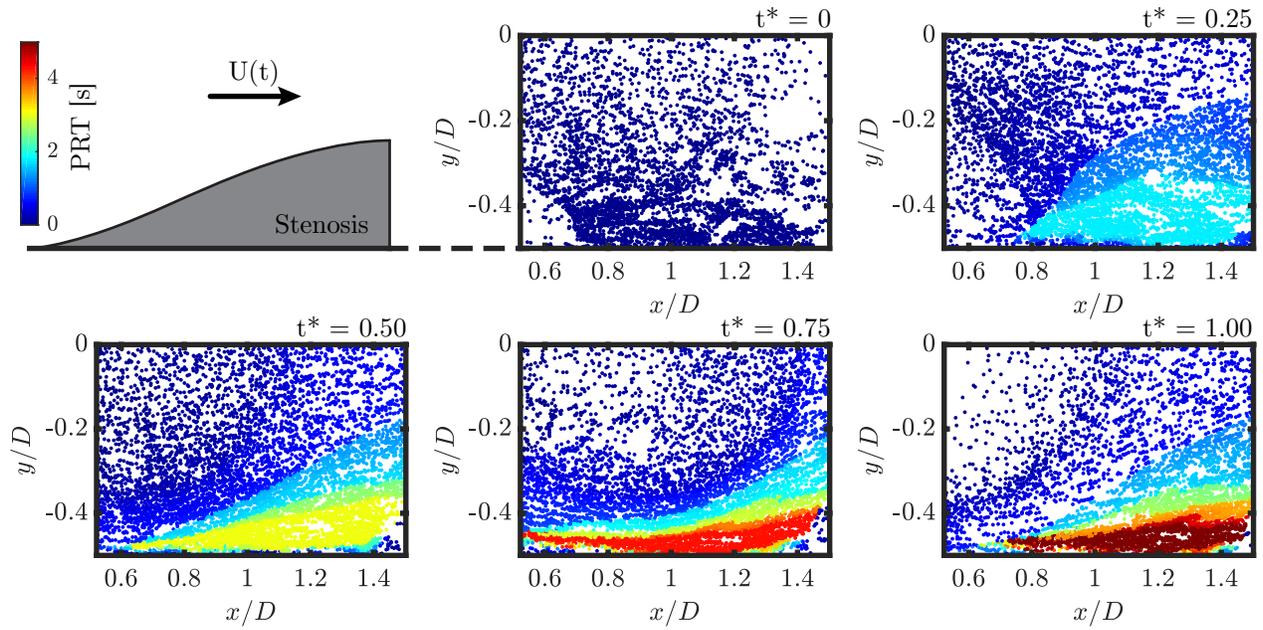
Figure 6: Flow through a stenosis model is tracked using echoLPT. Individual particle trajectories are mapped and labelled according to their trajectory through the measurement domain following the methods described by Jeronimo et al. (2019). Colour labels are assigned based on Figure 5(b). The pulsatile case in this example has $Re_m = 64$, $\alpha = 15$ and $\lambda = 1.0$.

Ultrasound images must be optimized for particle tracking: seeding concentration and power, frequency and gain of the incident and reflected sound waves each contribute to minimizing surface reflections and particle ambiguity. Regardless, the low signal-to-noise ratio of the images necessitates image preprocessing before particle detection and tracking can be executed. Background, smoothing and sharpening filters assist in isolating microbubbles that can be tracked and extended to map their entire trajectory. EchoLPT is capable of tracking thousands of unique flow tracers across hundreds of image frames. The ability to monitor particle-specific characteristics, like PRT, is of immense value to the medical community. PRT was measured for each microbubble that entered the region of interest and elucidates differences in pulsatile flow behaviour for increasing Re_m, α and λ. It was shown that pulsatility encouraged mixing into the near-wall region, while large velocity gradients increased particle turnover and decreased PRT.
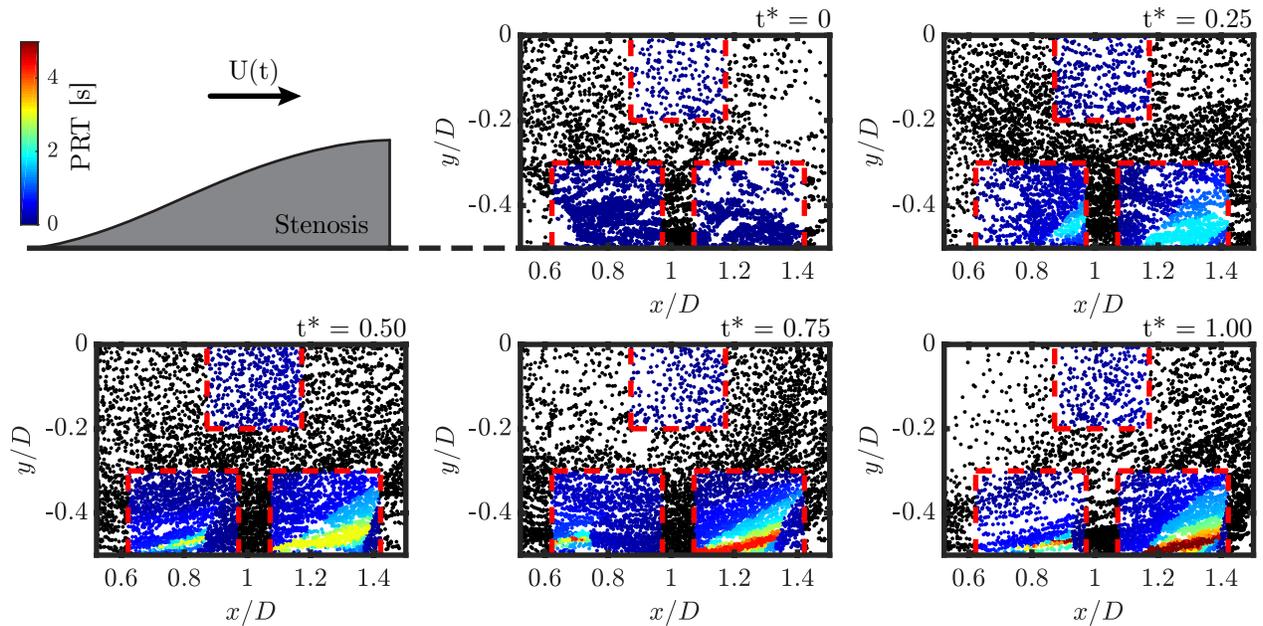
The technique remains grounded by the limitations and quality of ultrasound imaging. The field of view, depth of scan, dynamic range and streamwise resolution all limit the frame rate, while fluctuating bubble shape, strong surface reflections and loss of particles due to prolonged ultrasound exposure affect detection and tracking. While acquisition rates and image quality will inevitably improve with advancements of the underlying ultrasound technology, future studies will attempt to account for irregular particle image shape and incorporate existing UIV techniques to improve tracking (PIV+PTV).

Acknowledgements

(a) Instantaneous PRT of all particles

(b) Instantaneous PRT of particles in select regions of interest

Figure 7: PRT is extracted from a post-stenotic flow using echoLPT by mapping the trajectory of each particle that enters the measurement domain. Bubbles are coloured by the time they have spent in (a) the measurement domain or (b) any of three regions of interest (red dashed lines). Long PRT has been linked to plaque deposition *in vivo*. Particles outside the regions of interest are coloured black. These results are for a pulsatile flow with $Re_m = 64$, $\alpha = 15$ and $\lambda = 1.0$.
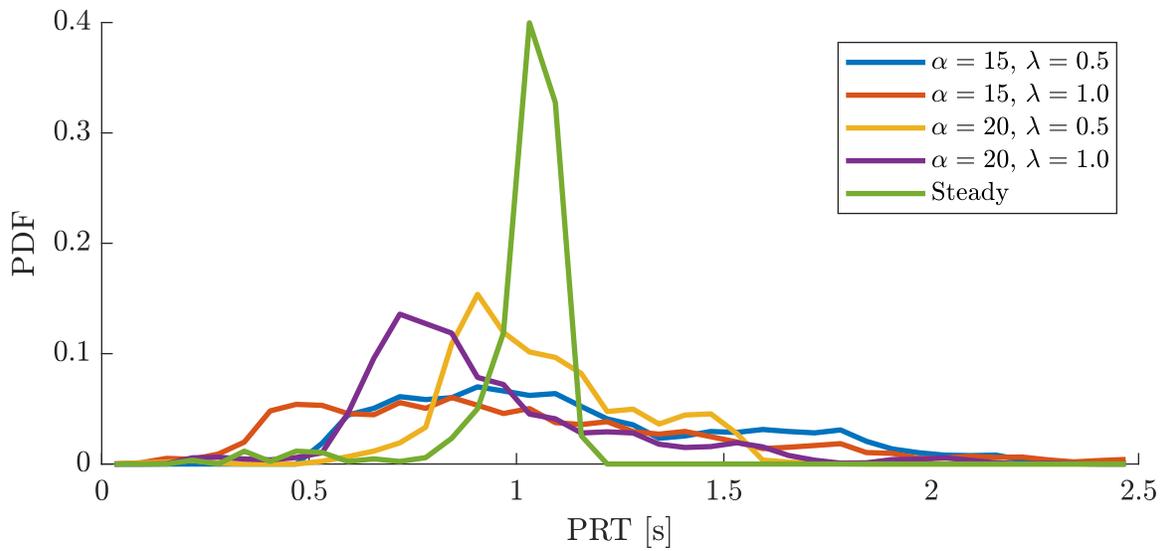
Figure 8: A tracer particle's PRT is a function of its trajectory. The distribution of red particle PRT reveal the effects of Womersley number (α) and amplitude ratio (λ) for unsteady flows at $Re_m = 64$.

(a) $\alpha = 15, \lambda = 0.5$

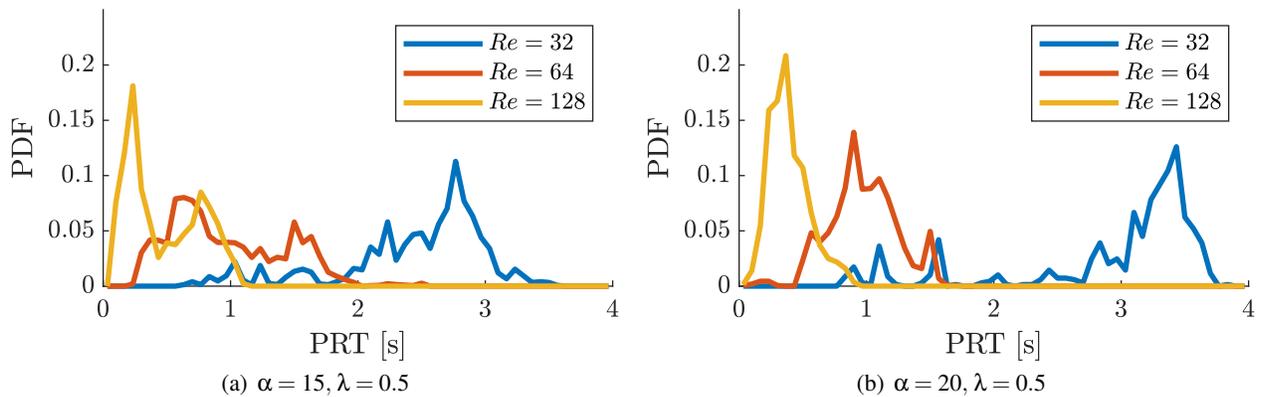(b) $\alpha = 20, \lambda = 0.5$

Figure 9: The probability density function of the PRT of red-labeled microbubbles revealing quantifiable differences between flows at (a) $\alpha = 15$ and (b) $\alpha = 20$ ($\lambda = 0.5$ for both). The same net volume through the stenosis geometry is compared at each Reynolds number and the trend of decreasing PRT with increasing Re_m is clear.

References

Ackermann D and Schmitz G (2016) Detection and tracking of multiple microbubbles in ultrasound b-mode images. *IEEE Transactions on Ultrasonics, Ferroelectrics, and Frequency Control* 63:72–82

Adamczyk AA and Rimai L (1988) 2-dimensional particle tracking velocimetry (PTV): Technique and image processing algorithms. *Experiments in Fluids* 6:373–380

Adrian RJ and Westerweel J (2011) *Particle Image Velocimetry*. Cambridge University Press

Crapper M, Bruce T, and Gouble C (2000) Flow field visualization of sediment-laden flow using ultrasonic imaging. *Dynamics of Atmospheres and Oceans* 31:233 – 245

Jeronimo MD, Zhang K, and Rival DE (2019) Direct Lagrangian measurements of particle residence time. *Experiments in Fluids* 60:72

Kim HB, Hertzberg JR, and Shandas R (2004) Development and validation of echo PIV. *Experiments in Fluids* 36:455–462

Niu L, Qian M, Yan L, Yu W, Jiang B, Jin Q, Wang Y, Shandas R, Liu X, and Zheng H (2011) Real-time texture analysis for identifying optimum microbubble concentration in 2-D ultrasonic particle image velocimetry. *Ultrasound in Medicine & Biology* 37:1280–1291

Ortiz SHC, Chiu T, and Fox MD (2012) Ultrasound image enhancement: A review. *Biomedical Signal Processing and Control* 7:419–428

Poelma C (2017) Ultrasound imaging velocimetry: A review. *Experiments in Fluids* 58:3

Raffel M, Willert CE, Scarano F, Käehler CJ, Wereley ST, and Kompenhans J (2018) *Particle Image Velocimetry: A Practical Guide*. Springer. 2 edition

Rosi GA and Rival DE (2018) A Lagrangian perspective towards studying entrainment. *Experiments in Fluids* 59:19

Sampath K, Harfi TT, George RT, and Katz J (2018) Optimized time-resolved echo particle image velocimetry– particle tracking velocimetry measurements elucidate blood flow in patients with left ventricular thrombus. *Journal of Biomechanical Engineering* 140:041010

Scarano F (2013) Tomographic piv: principles and practice. *Measurement Science and Technology* 24

Schanz D, Gesemann S, and Schröder A (2016) Shake-The-Box: Lagrangian particle tracking at high particle image densities. *Experiments in Fluids* 57:70

Song P, Trzasko JD, Manduca A, Huang R, Kadirvel R, Kallmes DF, and Chen S (2018) Improved super-resolution ultrasound microvessel imaging with spatiotemporal nonlocal means filtering and bipartite graph-based microbubble tracking. *IEEE Transactions on Ultrasonics, Ferroelectrics, and Frequency Control* 65:149–167

Tambasco M and Steinman DA (2003) Path-dependent hemodynamics of the stenosed carotid bifurcation. *Annals of Biomedical Engineering* 31:1054–1065

Walker AM, Scott J, Rival DE, and Johnston CR (2014) In vitro post-stenotic flow quantification and validation using echo particle image velocimetry (echo piv). *Experiments in Fluids* 55

Womersley J (1955) Method for the calculation of velocity, rate of flow and viscous drag in arteries when the pressure gradient is known.. *Journal of Physiology* pages 553–563

Zhang F, Lanning C, Mazzaro L, Barker AJ, Gates PE, Strain WD, Fulford J, Gosling OE, Shore AC, Bellenger NG, Rech B, Chen J, Chen J, and Shandas R (2011) In vitro and preliminary in vivo validation of echo particle image velocimetry in carotid vascular imaging. *Ultrasound in Medicine & Biology* 37:450–464

Zheng H, Liu L, Williams L, Hertzberg JR, Lanning C, and Shandas R (2006) Real time multicomponent echo particle image velocimetry technique for opaque flow imaging. *Applied Physics Letters* 88:261915